



PCCP

**Interfacial Structural Crossover and Hydration
Thermodynamics of Charged C60 in Water**

Journal:	<i>Physical Chemistry Chemical Physics</i>
Manuscript ID	CP-ART-08-2018-005422.R1
Article Type:	Paper
Date Submitted by the Author:	27-Sep-2018
Complete List of Authors:	Sarhangi, Setare; Iran University of Science and Technology, Chemistry Waskasi, Morteza; Arizona State University College of Liberal Arts and Sciences, School of Molecular Sciences Hashemianzadeh, Seyed Majid; Molecular Simulation Research Laboratory, Department of Chemistry, Iran University of Science & Technology, Matyushov, Dmitry; Arizona State University, Chemistry and Biochemistry

SCHOLARONE™
Manuscripts



Cite this: DOI: 10.1039/xxxxxxxxxx

Interfacial Structural Crossover and Hydration Thermodynamics of Charged C₆₀ in Water[†]

Setare Mostajabi Sarhangi^a, Morteza M. Waskasi,^b Seyed Majid Hashemianzadeh^a, and Dmitry V. Matyushov^{*c}

Received Date

Accepted Date

DOI: 10.1039/xxxxxxxxxx

www.rsc.org/journalname

Classical molecular dynamics simulations of hydration thermodynamics, structure, and dynamics of water in hydration shells of charged buckminsterfullerenes are presented in this study. Charging of fullerenes leads to a structural transition in the hydration shell, accompanied by creation of a significant population of dangling O-H bonds pointing toward the solute. In contrast to the well accepted structure-function paradigm, this interfacial structural transition causes nearly no effect on either the dynamics of hydration water or on the solvation thermodynamics. Linear response to the solute charge is maintained despite significant structural changes in the hydration shell, and solvation thermodynamic potentials are nearly insensitive to the altering structure. Only solvation heat capacities, which are higher thermodynamic derivatives of the solvation free energy, indicate some sensitivity to the local hydration structure. We have separated the solvation thermodynamic potentials into direct solute-solvent interactions and restructuring of the hydration shell and analyzed the relative contributions of electrostatic and nonpolar interactions to the solvation thermodynamics.

1 Introduction

We present new computational evidence of the disconnect between the interfacial dynamics and interfacial structure. We have simulated different charge states of buckminsterfullerene C₆₀^z carrying different net charges, from $z = +1$ to $z = -4$. The simulation results clearly show that hydration water undergoes a structural crossover at $z = -3$ and $z = -4$ without significant effect on the dynamics of water in the interface.

The structure-function relation is viewed as a cornerstone for understanding complexity in such different fields as material science and biology. In its basics, it looks for a reduction of complex phenomena to the structural information, that is to the spatial organization of the atoms. The structure can be fully derived from the interatomic interactions, but this information is not sufficient to completely characterize the dynamics, which require forces. Even though forces are derived from the potentials, the connection between the dynamics and structure might be less direct than is often assumed. A pedagogical example is the case of a van der

Waals liquid, which is constructed by combining hard-core repulsion with a mean-field attraction, i.e., an infinitesimally shallow potential with an infinite range providing a uniform cohesive energy of a bulk liquid.^[1,2] Such a mean-field attraction is obviously very significant for the thermodynamics of the liquid, but exerts no forces on the molecules and does not affect the liquid dynamics. In a more general sense, the range and the strength of the interaction potential produce different effects on the statistics and structure on the one hand and on the dynamics and relaxation on the other hand: weak and long-ranged interaction potentials can significantly affect the structure and thermodynamic functions, but a steeply-altering potential can produce a stronger effect on the dynamics because of the stronger forces involved.

While there are no general grounds to doubt this reasoning, there are not many examples clearly showing a disconnect between structural changes and the corresponding changes in dynamics. In some areas of condensed matter science, the dynamics-structure connection is viewed as quite plausible, and the evidence for it is actively sought for. For instance, many glass formers close to their glass transition show rapid slowing of the dynamics,^[3] which is connected to either the run-off of the configurational entropy through the Adam-Gibbs theory^[4,5] or to a still hypothesized growth of spatial (structural) correlations.^[6,7] Both ideas advocate structural change underlying sharp slowing of the dynamics. Likewise, interfacial dynamics of water are often linked to the interfacial structure and the network of hydro-

^a Molecular Simulation Research Laboratory, Department of Chemistry, Iran University of Science and Technology, Tehran 16846-13114, Iran

^b School of Molecular Sciences, Arizona State University, PO Box 871504, Tempe, AZ 85287-1504

^c Department of Physics and School of Molecular Sciences, Arizona State University, PO Box 871504, Tempe, AZ 85287-1504; E-mail: dmitrym@asu.edu

[†] Electronic Supplementary Information (ESI) available: [details of any supplementary information available should be included here]. See DOI: 10.1039/b000000x/

gen bonds in the hydration shell. In that paradigm, measuring the interfacial dynamics is viewed as a way of probing the interfacial structure.^[8,9] The latter is particularly significant for the problem of hydrophobic solvation where structure of water in the interface is often related to entropic effects observed in solvation of nonpolar solutes.^[10,11]

Despite structural transition in the interface observed in the simulations, we find that solvation thermodynamics of C_{60}^z , $z = -4, \dots, +1$ follows linear solvation remarkably well. This is surprising because the linear response approximation is constructed based on the assumption that the solute-solvent interaction does not alter the structure of the solvent.^[12,13] Since electrostatic solvation dominates for highly negative solutes for which transition occurs, the overall solvation thermodynamics is not sensitive to the local structural change. We therefore demonstrate that both the solvation thermodynamics and interfacial dynamics are decoupled from local structural crossovers in the interface. Only higher thermodynamic derivatives of the solvation free energy, such as solvation heat capacity, are noticeably affected by the structural transition and can report on the structural transition in the interface. We present detailed calculations of the electrostatic and non-polar (Lennard-Jones) components of solvation accounting for structural reorganization of the hydration shell and its effect on the energy and heat capacity of solvation.

2 Solvation thermodynamics

Thermodynamic perturbation theories^[14–18] of solvation thermodynamics seek to separate the intermolecular solute-solvent interaction into a reference potential responsible for repulsion from the solute's core and a slowly varying perturbation interaction u_{0s} (“0” for the solute and “s” for the solvent).^[19–22] We follow here this tradition and define the hard-sphere (HS) repulsive core^[16,19,23] of the solute with the potential function u_{0s}^{HS} . The reference potential (Hamiltonian) H_0 is then the sum of u_{0s}^{HS} and all solvent-solvent interactions U_{ss}

$$H_0 = u_{0s}^{\text{HS}} + U_{ss}. \quad (1)$$

In other words, the reference system is the pure solvent and the hard-sphere core of the solute. Since the hard-sphere potential u_{0s}^{HS} is purely geometrical, thermal fluctuations do not alter the solute-solvent part of the reference potential and $\delta H_0 = \delta U_{ss}$. We will use this property below in the calculation of thermodynamic functions for solvation.

The hard-sphere potential u_{0s}^{HS} cuts all components of the solute solvent interaction within its hard core. Therefore, the solute-solvent interaction $u_{0s} = u_{0s}^{\text{LJ}} + u_{0s}^{\text{E}}$ is the sum of the dispersive Lennard-Jones (LJ) potential u_{0s}^{LJ} and the electrostatic interaction u_{0s}^{E} taken outside of the hard core. For the LJ potential, this assignment corresponds to the Barker-Henderson perturbation theory,^[16] as we discuss in more detail below. The excess chemical potential of solvation due to solute-solvent long-ranged, LJ and electrostatic, interactions is given by Widom's formula^[24]

$$\beta\mu_{0s} = -\ln \left\langle e^{-\beta u_{0s}} \right\rangle_0. \quad (2)$$

Here, $\langle \dots \rangle_0$ denotes an ensemble average in the reference state and $\beta = (k_{\text{B}}T)^{-1}$ is the inverse temperature.

An alternative formula for μ_{0s} is offered by thermodynamic integration.^[12] One scales the solute-solvent interaction with the parameter $0 \leq \lambda \leq 1$ to produce the Hamiltonian

$$H_\lambda = H_0 + \lambda u_{0s}, \quad (3)$$

where $\lambda = 0$ leads to H_0 in Eq. (1). The Gibbs ensemble average with the Hamiltonian H_λ is then specified with the subscript λ in the angular brackets, $\langle \dots \rangle_\lambda$. In this approach, the solvation chemical potential is the reversible work of the “charging” process in which the long-ranged solute-solvent potential u_{0s} is continuously turned on

$$\mu_{0s} = \int_0^1 \langle u_{0s} \rangle_\lambda d\lambda. \quad (4)$$

The energy of solvation follows from the thermodynamic relation

$$e = (\partial(\beta\mu_{0s})/\partial\beta)_V. \quad (5)$$

It can be separated into the energy of the solute-solvent interaction e_{0s} and the term e_{ss} describing the modification of the solvent-solvent interaction energy induced by the solute^[25–27]

$$e = e_{0s} + e_{ss}, \quad (6)$$

where

$$e_{0s} = \langle u_{0s} \rangle_1 \quad (7)$$

and $\langle \dots \rangle_1$ corresponds to $\lambda = 1$, when the full solute-solvent interaction potential is turned on in the system Hamiltonian. The representation of the thermodynamic functions in terms of these averages is preferable for numerical applications since this is the ensemble produced by MD simulations discussed below. For brevity, we will drop the subscript from the averages corresponding to $\lambda = 1$, thus adopting $\langle \dots \rangle = \langle \dots \rangle_1$.

From Eq. (2) one gets^[25,26]

$$e_{ss} = \langle H_0 \rangle - \langle H_0 \rangle_0. \quad (8)$$

The solvent restructuring energy is, therefore, the change in the interactions between the solvent molecules introduced by turning the long-ranged solute-solvent interactions on. Since H_0 includes the HS repulsion u_{0s}^{HS} with diverging energy, an alternative fluctuation relation is more convenient for applications. By applying λ -scaling of the solute-solvent interaction according to Eq. (3), one obtains^[25,26]

$$e_{ss} = -\beta \int_0^1 \langle \delta u_{0s} \delta U_{ss} \rangle_\lambda d\lambda, \quad (9)$$

where δu_{0s} and δU_{ss} denote the deviations from the corresponding average values. Note that $\delta H_0 = \delta U_{ss}$ was used to arrive at Eq. (9).

The term e_{ss} was also designated as the “solvent reorganization term”^[25,27] or “solvent reorganization energy”^[11] Since both terms can lead to confusion with the “solvent reorganization energy” much earlier reserved for the free energy entering the free energy barrier for electron transfer reactions,^[28] we avoid using this terminology here (note that the “solvent reorganization en-

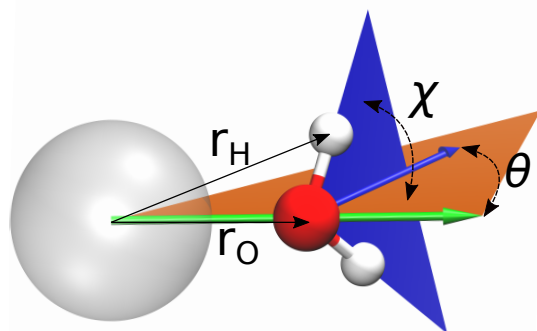


Fig. 1 Schematic representation of the water molecule in the hydration shell of C_{60}^z : r_O is the distance between the oxygen atom and the center of the solute, r_H is the distance between the hydrogen atom and the center of the solute, θ is the angle between water's dipole (blue arrow) and the radial direction (green arrow), and χ is the angle between the planes of the water molecule (blue plane) and that of the dipole moment and the radial direction (orange plane).

tropies" in refs 29 and 11 refer to quite distinct properties).

The heat capacity of solvation follows from the second derivative of the excess chemical potential

$$C_V/k_B = -\beta^2 \left(\partial^2 (\beta \mu_{0s}) / \partial \beta^2 \right)_V. \quad (10)$$

Applying this derivative to Eqs. (6) and (8), one obtains

$$\begin{aligned} C_V/k_B &= \beta^2 \langle (\delta u_{0s} + \delta U_{ss})^2 \rangle - \beta^2 \langle \delta U_{ss}^2 \rangle_0 \\ &= \beta^2 \langle (\delta u_{0s})^2 \rangle + 2\beta^2 \langle \delta u_{0s} \delta U_{ss} \rangle + \Delta C_{ss}/k_B. \end{aligned} \quad (11)$$

In the second line of this equation, $\Delta C_{ss}/k_B = \beta^2 \langle \delta U_{ss}^2 \rangle - \beta^2 \langle \delta U_{ss}^2 \rangle_0$ is the change of the heat capacity of the solvent due to the long-ranged solute-solvent interactions. Each of these variances scales linearly with the number of solvent particles in their leading terms. Since C_V is intensive, these $\propto N$ terms should identically cancel out in their difference. The intensive term, ΔC_{ss} , remaining after the cancellation of two macroscopic extensive terms, can potentially be affected by finite-size effects when evaluated from numerical simulations. We show below that this is indeed the case, and we evaluate this term for the electrostatic component of the heat capacity by extrapolating the finite-size simulation results to $N \rightarrow \infty$.

The definition of the heat capacity used here is one of several thermodynamic routes to the solvation heat capacity from taking two derivatives of the system energy/enthalpy in terms of the number of solutes and temperature while keeping volume/pressure constant.^[30] Since four such combinations can be produced, there are four thermodynamic heat capacities C_{ab} , where $a, b = P, V$. In our simulations, NVT ensemble was used and C_V in Eq. (11) corresponds to the thermodynamic heat capacity C_{VV} . Corrections are still required if thermodynamic transfer heat capacities are used for the experimental input.^[30,31] We also

stress that μ_{0s} considered here is not the full solvation chemical potential. The highly nonlinear^[32] free energy of inserting the repulsive core of the solute into the liquid (free energy of cavity formation^[22,31,33]) is excluded from the analysis by our choice of the reference system. We focus only on solvation due to electrostatic and long-ranged LJ interactions and on the alteration of this solvation thermodynamics by the structural crossover in the hydration shell.

Below, we apply this formalism to the electrostatic and LJ components separately, but first turn to the structural changes in the interface of C_{60}^z found in MD simulations while altering the charge z of the fullerene solute. The main result of our study is a remarkable insensitivity of the solvation thermodynamics combining the electrostatic and LJ components to local structural changes in the hydration shell in the entire range of charges studied here.

3 Results

Simulation protocol. We have performed molecular dynamics simulations of the charged states of C_{60}^z by using NAMD software suite.^[34] The details of the simulation protocol can be found in the Electronic Supplementary Information (ESI[†]), along with additional data analysis. Briefly, the simulation performed in the NVT ensemble involved 2413 SPC/E waters in equilibrium with a single C_{60}^z solute. The typical length of the simulation trajectory was 110 ns. The distribution of partial atomic charges in charged fullerenes was calculated by DFT and not altered continuously, as is often done in solvation studies.^[35,36] We, therefore, do not study solvation of partial molecular charges here and instead focus on whole charges in the range $-4 \leq z \leq 1$.

A number of parameters have been analyzed to characterize changes in the structure of the hydration layers with charging of the solute. In order to navigate in the parameters considered here, Fig. 1 illustrates a water molecules in the hydration shell close to C_{60}^z with distances from the oxygen, r_O , and from the hydrogen, r_H , to the center of the solute. The distribution of those is characterized below through the pair distribution functions (PDFs). In addition, the orientation of the water molecule in the interface is characterized by two angles: the angle θ between its dipole moment and the radial direction and the angle χ between two planes: the plane formed by the dipole moment and the radial direction and the plane of the water molecule.

Interfacial structure. The first signature of the structural transition of the hydration shell is seen from PDFs shown in Fig. 2. Two sets of solute-water functions are presented: the solute-oxygen PDFs (Fig. 2a) and solute-hydrogen PDFs (Fig. 2b). The solute-oxygen PDFs show that the solvent shell softens with the fullerene charge changing from $z = 1$ to $z = -2$, with nearly no change between $z = 1$ and $z = 0$. The peak of the oxygen PDF with the position r_O^{\max} gets lower for $z = -1$ and $z = -2$, which corresponds to a less structured hydration shell. However, this trend is reversed at $z = -3$ and -4 , and the oxygen peak gets sharper and shifts to smaller distances, signaling a more structured shell. The first peak of the hydrogen distribution nearly coincides with that for oxygen at $|z| \leq 1$, which implies that waters are mostly in plane of the fullerene-water dividing surface.^[37,38] At $z \leq -2$, one observes a substantial growth of the hydrogen peak (Fig. 2b)

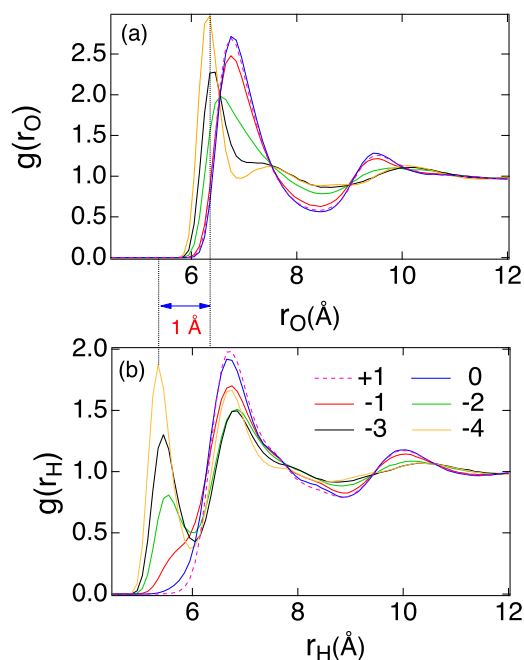


Fig. 2 Radial distribution functions for oxygens (a) and hydrogens (b) of the water molecules in the hydration shell of C_{60}^z at 300 K. Different charge state z are listed in the plots. The distance of 1 Å between the oxygen and hydrogen peaks at $z = -4$ is shown in the plot to indicate that the OH bond of hydration water points to the center of C_{60}^{-4} in this charge configuration.

at the distance ≈ 1 Å shorter than the oxygen peak. This is a signature of dangling OH bonds pointing toward the solute.^[39–41] It is accompanied by the disruption of the hydrogen-bond network in the hydration shell resulting in the higher density of the shell. Interfacial water turns into a layered structure commonly observed at interfaces with hydrophilic and charged substrates.^[42,43]

The parameters of the first hydration layer are summarized in Table 1. We list the number of first-shell waters N_s^l and the fraction of the dangling bonds $n_s^{\text{OH}} = N_s^{\text{OH}}/N_s^l$, where N_s^{OH} is the total number of dangling bonds in the first hydration shell. In addition, the position of the first peak, r_O^{max} , and of the first minimum, r_O^{min} , of the solute-oxygen PDF $g_O(r)$ (Fig. 2a) are listed. The first shell

Table 1 Parameters of the first hydration shell of C_{60}^z at 300 K: the number of first-shell waters N_s^l , the fraction of dangling bonds n_s^{OH} , the number of hydrogen bonds per water molecule n_{HB} , and the positions of the first peak, r_O^{max} , and of the first minimum, r_O^{min} of the solute-oxygen PDF (Å).

z	N_s^l	n_s^{OH}	n_{HB}^a	r_O^{max}	r_O^{min}
1	79.6		3.34	6.75	8.45
0	81.0		3.23	6.75	8.45
-1	82.1		3.11	6.75	8.45
-2	83.4	0.11	3.02	6.55	8.45
-3	38.8	0.39	2.42	6.45	6.95
-4	42.7	0.42	2.36	6.35	6.95

^aThe number of hydrogen bonds per water molecule in bulk SPCE is $n_{\text{HB}} = 3.6$ at 300 K.^[44]

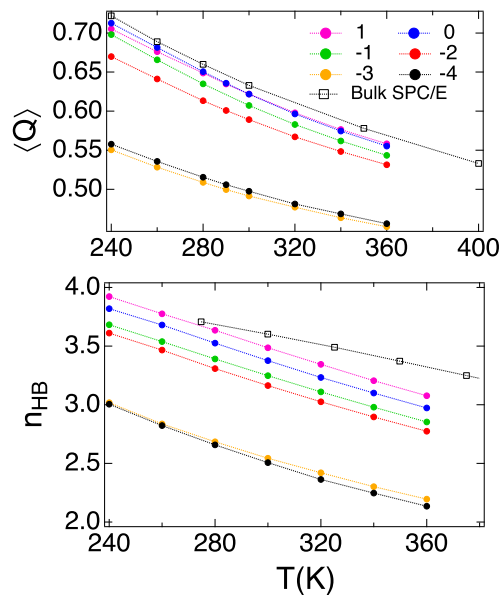


Fig. 3 Upper panel: average tetrahedral order parameter $Q(T) = \langle Q \rangle$ in the first hydration shell of C_{60}^z as a function of temperature in all charge states z indicated in the plot. Also shown are the results for $Q(T)$ for bulk SPC/E water^[49] (open points). Lower panel: the average number of hydrogen bonds per water molecule in the first hydration shell n_{HB} . Open points refer to bulk SPC/E water.^[44]

is defined throughout below as all positions of the water oxygens within the distance $r \leq r_O^{\text{min}}$ corresponding to the first minimum of the solute-water PDF (Fig. 2 and Table 1).

The picture of the charge-induced structural transition in the hydration shell is further supported by all structural parameters we have calculated to provide details of the positional and orientational arrangement of hydration waters. Since we anticipate that the appearance of a large density of dangling OH bonds should disrupt the hydrogen-bond network, we have calculated the tetrahedral order parameter for the water molecules in the hydration shell^[45–48]

$$Q = 1 - \frac{3}{8} \sum_{i=1}^3 \sum_{j=i+1}^4 (\cos \theta_{ij} + 1/3)^2. \quad (12)$$

This parameter is specified by the angle θ_{ij} formed by a target molecule with its four nearest neighbors i and j . Fully ordered tetrahedral structure yields $\langle Q \rangle = 1$, and $\langle Q \rangle = 0$ describes the state of orientational disorder.

We show in the upper panel of Fig. 3 the average tetrahedral parameter $Q(T) = \langle Q \rangle$ at different temperatures calculated for the first hydration shell of C_{60}^z . Tetrahedral order is generally reduced^[50] in the hydration shell compared to bulk SPC/E water^[49] (open points in Fig. 3). The order is progressively reduced with increasing the solute charge (as is also found for monovalent and divalent cations^[51]), but the transition to $z = -3$ and $z = -4$ shows a much deeper drop of tetrahedral order. The distributions $P(Q)$ are also quite revealing showing a shift of the highest peak of $P(Q)$ to lower values of Q (less order) when increasing the negative charge of the fullerene (Fig. 4). The effect of temperature

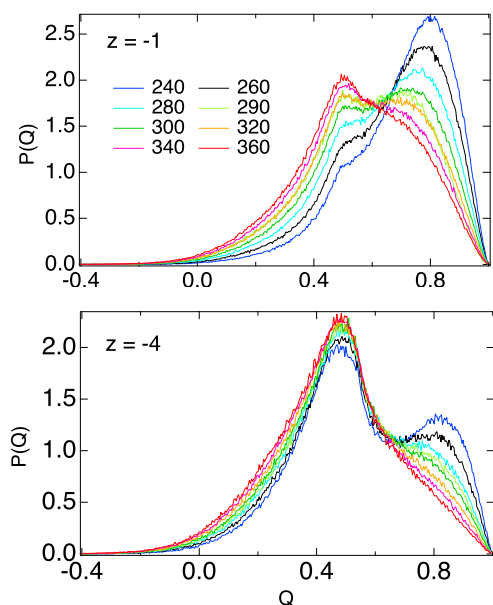


Fig. 4 Distributions of the tetrahedral order parameter Q (Eq. (12)) for C_{60}^z at $z = -1$ (upper panel) and $z = -4$ (lower panel). The order parameter is calculated in the first hydration shell defined by distances r_O less than the distance to the first minimum of the oxygen PDF (Figs. 1 and 2). The results of calculations are shown at different temperatures indicated in the plot.

on $P(Q)$ is significant for low charges due to breaking of tetrahedral order by thermal agitation.^[48] In contrast, tetrahedral order is already broken by the electrostatic field of the solute for $z \leq -3$, and increasing temperature makes little effect on the main peak and just lowers the high-order wing of the distribution (Fig. 4).

The lower panel in Fig. 3 presents the number of hydrogen bonds n_{HB} per water molecule in the first hydration shell of C_{60}^z calculated according to the typical geometric definition of a hydrogen bond.^[52] The results for the first hydration shell are compared to bulk SPC/E water^[44] (open points in Fig. 3). We observe a small gap in the number of hydrogen bonds between waters in contact with the neutral C_{60} compared to the bulk, which, however, widens with increasing temperature. The results for the neutral C_{60} are in agreement with previous simulations.^[37,44] The issue of the number of hydrogen bonds in hydration shells was also studied by fitting analytical two-state solvation models to the hydration thermodynamics.^[53,54] Our calculations support the view of weakening hydrogen bonds^[54] in contrast to their strengthening.^[53] Charging fullerenes further lowers the number of hydrogen bonds (Table 1), and the trend for n_{HB} is in general accord with $Q(T) = \langle Q \rangle$.

The loss of tetrahedral order and breaking of hydrogen bonds are accompanied by increased ordering of the shell dipoles along the local electric fields, which, as the charge is increased, is less hindered by hydrogen bonds among the water molecules. The cooperative nature of hydrogen bonds leads to a sharp and distinct alteration of the orientational distribution with increasing $|z|$. In order to characterize changes in the orientational structure, we have considered two first Legendre polynomials of the

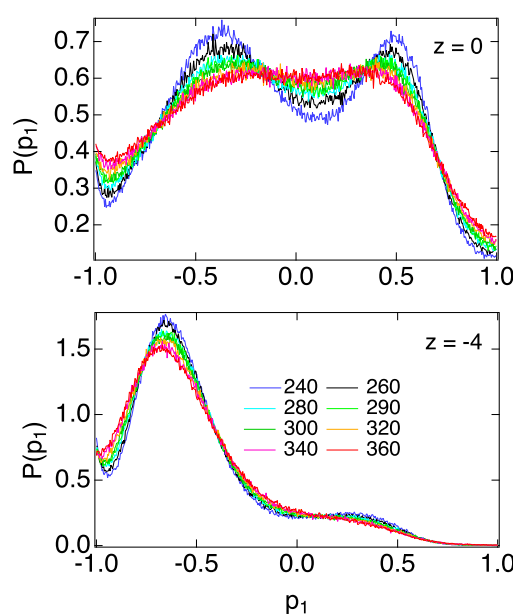


Fig. 5 Distribution of the order parameter p_1 ($\ell = 1$ in Eq. (13)) of the first hydration shell of C_{60}^z at changing temperature (the definition of the first hydration shell is the same as in Fig. 4). The upper panel shows the results for $z = 0$ and the lower panel refers to $z = -4$; the temperatures are listed in plot.

scalar product between the unit vector of the dipole moment $\hat{\mu}$ with the unit vector \hat{r} of the radius vector \mathbf{r} connecting the solute's center to the oxygen atom to which the dipole moment is assigned. The orientational order parameter is defined in terms of the Legendre polynomial $P_\ell(x)$ as follows

$$p_\ell(\mathbf{r}) = P_\ell(\hat{\mu} \cdot \hat{r}). \quad (13)$$

The plots of the distribution functions for $p_1(\mathbf{r})$ when \mathbf{r} is in the first hydration shell of C_{60}^z are shown for $z = 0$ and $z = -4$ in Fig. 5 (the distributions for other charges can be found in ESI[†]). We find that a broad and somewhat skewed distribution of dipolar orientations around a nonpolar solute^[37,38,55] is replaced by a highly asymmetric distribution with its peak representing the preferential orientation of the dipoles pointing toward the solute at $\theta = 130^\circ$, also found in previous simulations of soft-repulsive^[44] and charged^[56] spherical solutes. Given the HOH angle of 104° , this average value of θ implies that one of OH bonds is directed nearly straight toward the center of the solute, which is consistent with the PDFs shown in Fig. 2.

The dramatic change in the orientation of the water dipoles in the shell at $z = -3, -4$ is also accompanied with the rotation of the plane of the water molecules. The distributions of the angle χ (Fig. 1) at $z = 0, -1$ are peaked at $\chi \approx 90^\circ$ (Fig. 6). The water molecules in the hydration shell are mostly positioned parallel to the dividing interfacial surface, as was found in many previous studies of water in contact with hydrophobic surfaces.^[39–41,57] On the contrary, the appearance of the dangling OH bonds at $z = -3, -4$ forces the water molecules to rotate into the plane of the dipole moment and the radius-vector ($\chi \approx 0$ or $\chi \approx 180^\circ$ in

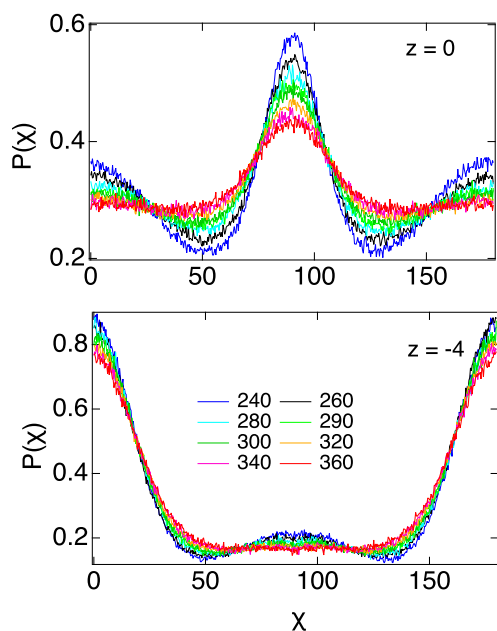


Fig. 6 Distribution of angle χ (Fig. 1) of water molecules in the hydration shell of C_{60}^z at changing temperature. The upper panel shows the results for $z = 0$ and the lower panel refers to $z = -4$.

Fig. 6).

To summarize, the evidence presented in Figs. 2–6 shows a structural transition of the hydration shell changing from a structure specific for interfaces of water with hydrophobic surfaces/solutes to a shell with broken hydrogen bonds released as dangling OH pointing toward the solute (with the population of ≈ 0.4 for $z = -3, -4$, Table 1). While signatures of this new structural order are seen already at $z = -2$, the most pronounced structural change appears for $z = -3, -4$. The new structure persists at all temperatures studied here and is not strongly affected by temperature. One anticipates that the appearance of dangling bonds in hydration shells of charged fullerenes should have spectroscopic evidence.^[58–60] Our next focus is on solvation thermodynamics of fullerenes and on the dynamics of the solute-solvent interaction and the dynamics of hydration water.

Solvation. The solvation thermodynamics is often described in the Gaussian^[32,61] or linear response^[12,62] approximation in which the thermodynamic integration for the excess chemical potential is replaced by the expansion in terms of two first non-vanishing cumulants

$$\mu_{0s} = e_{0s} + (\beta/2)\langle(\delta u_{0s})^2\rangle, \quad (14)$$

where

$$e_{0s} = \langle u_{0s} \rangle. \quad (15)$$

In the second summand of Eq. (14), the cross-correlations between the fluctuations of electrostatic and LJ interactions, $\langle \delta u_{0s}^E \delta u_{0s}^{LJ} \rangle$, can often be neglected (which is the case with our MD simulations). When such a decoupling approximation is adopted, one can write the above equation for each component

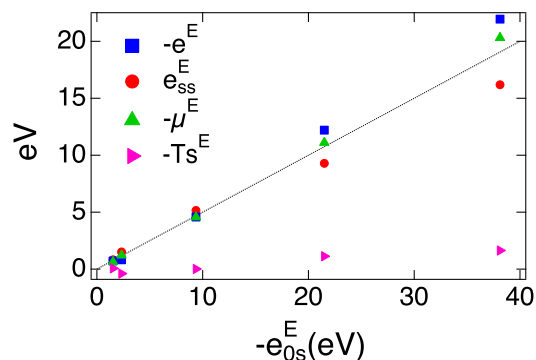


Fig. 7 Thermodynamic potentials of electrostatic solvation of C_{60}^z in different charge states z versus negative of the average solute-solvent electrostatic interaction energy e_{0s}^E at $T = 300$ K. The points are MD results and the dashed line shows the expectation of the linear response approximation, $\mu_{0s}^E = (1/2)e_{0s}^E$, Eq. (17).

$$\mu_{0s}^s, \quad s = E, LJ$$

$$\mu_{0s} = \mu_{0s}^E + \mu_{0s}^{LJ}. \quad (16)$$

The problem of ion solvation is further simplified by a nearly universally observed^[35,63,64] quadratic scaling of the average solute-solvent interaction with the solute charge, $\langle u_{0s}^E \rangle_\lambda \propto \lambda^2$. This scaling significantly simplifies the solvation thermodynamics for the electrostatic component. The solvation thermodynamic potentials are given by approximate, but often highly accurate, relations^[64]

$$\mu_{0s}^E = \frac{1}{2}e_{0s}^E, \quad e_{0s}^E = -\beta\langle(\delta u_{0s}^E)^2\rangle, \quad (17)$$

where the electrostatic solute-solvent interaction energy is

$$e_{0s}^E = \langle u_{0s}^E \rangle. \quad (18)$$

The same quadratic scaling applies to the component $\langle \delta u_{0s}^E \delta U_{ss} \rangle_\lambda$ in Eq. (9), which simplifies the equation for the solvent restructuring energy to the following form

$$e_{ss}^E = -(\beta/2)\langle \delta u_{0s}^E \delta U_{ss} \rangle. \quad (19)$$

From Eqs. (6) and (17), one derives the expression for the entropy of electrostatic solvation

$$Ts^E = \mu_{0s}^E + e_{ss}^E. \quad (20)$$

Equation (20) provides access to e_{ss}^E from experimentally accessible thermodynamic solvation functions.

The results of calculations according to Eqs. (17)–(20) are listed in Table 2 and shown by points corresponding to charged states of C_{60}^z in Fig. 7. The dependence $\mu_{0s}^E(z)$ is shown in Fig. S12 in the ESI[†]. We find that all thermodynamic functions for electrostatic solvation follow the quadratic $\propto z^2$ scaling with the solute charge. Further, the average solute-solvent interaction energy e_{0s}^E displays asymmetry in respect to the sign flip $z = 1 \rightarrow z = -1$, which is a well-documented^[65] result for ionic solvation related to asymmetry of the molecular charge in the water molecule.^[66–68] Note, however, that this asymmetry has

mostly been reported for much smaller ions typically used for electrolytes, and we find here that this rule can be extended to much larger C_{60}^z solutes. We also find, similarly to our previous studies,^[69,70] a curious proximity between $-\mu_{0s}^E$ and the energy of solvent's restructuring e_{ss}^E

$$-\mu_{0s}^E \approx e_{ss}^E. \quad (21)$$

This empirical results holds less accurately for C_{60}^z studied here compared to surface solvation of C_{180} .^[70]

The near cancellation between two summands in Eq. (20) is difficult to describe by analytical models since it, in fact, represents a cancellation between two-solvent microscopic correlations entering μ_{0s}^E with three-solvent correlations required to calculate e_{ss}^E .^[71] Since these are correlations between the solvent particles in the vicinity of the solute, one in fact has to deal with three-particle, solute-solvent-solvent correlations for μ_{0s} and with the corresponding four-particle correlations for e_{ss} .^[15,72,73] Numerical errors of subtracting two large numbers have potentially contributed to the unexpected positive value of T_s^E for $z = -1$ (Table 2). Microscopic models dealing with high-order correlations involving molecular orientations have not been developed, and even formulating approximations for higher-order distribution functions currently presents a formidable theoretical challenge.^[15] Considering solvation of multipoles of different order might provide a helpful initial insight into molecular correlations contributing to each term in Eq. (20) since much less pronounced cancellation between those two terms was found for dipolar solvation, as discussed in Ref. 69.

Relations between thermodynamic solvation functions in Eqs. (11), (17), and (19) allow us to write the electrostatic heat capacity in the closed form

$$\left(\frac{C_V^E - \Delta C_{ss}^E}{k_B} - 2\beta\left(\mu_{0s}^E + 2e_{ss}^E\right)\right) \approx -2\beta e_{ss}^E, \quad (22)$$

where Eq. (21) was applied in the second approximate equality. Since $e_{ss}^E > 0$ (Table 2), the linear-response theory suggests that the heat capacity from direct electrostatic solute-solvent interactions is negative and is roughly proportional to the magnitude of the solvent restructuring energy.

The complexity of calculations of solvation heat capacity is well illustrated by Table 3. Its component due to changes in the solvent structure produced by the solute-solvent electrostatics, ΔC_{ss}^E , was calculated by subtracting $\langle \delta U_{ss}^2 \rangle(0)$ at $z = 0$ from $\langle \delta U_{ss}^2 \rangle(z)$ at $z \neq 0$

$$\Delta C_{ss}^E/k_B = \beta \langle \delta U_{ss}^2 \rangle(z) - \beta \langle \delta U_{ss}^2 \rangle(0). \quad (23)$$

The result of this procedure strongly depends on the system size, and the values reported in Table 3 were calculated by extrapolating to $N \rightarrow \infty$. The change of the solvent heat capacity $\Delta C_{ss}/k_B$ is positive (Table 3) and with the magnitude close to that of $-2\beta e_{ss}^E$ in Eq. (22). The resulting heat capacity of electrostatic interactions comes from mutual cancellation of two large contributions, and it changes sign as a function of the solute charge.

Comparison of simulated heat capacities to observations is not easy to establish. The overall heat capacities of aqueous electrolytes can be either positive or negative,^[74] but experiment

does not have access to individual ions. In addition, all components, the cavity formation thermodynamics, electrostatics, and LJ interactions, have to be included in a complete analysis. Previous simulations of heat capacity of aqueous electrolytes^[36] indicated that heat capacities of monovalent cations and anions can carry opposite signs: positive heat capacity for cations and negative heat capacity for anions. We also find this sign switch here, but it is followed by another change of sign for $z < -2$. This second sign change is caused by the collapse of the hydration shell at higher charges (Fig. 2), which leads to a significant increase of ΔC_{ss}^E given by Eq. (23).

We now turn to the LJ component of solvation. The average solute-solvent interaction energy is directly calculated from the simulation trajectories as an ensemble average

$$e_{0s}^{LJ} = \langle u_{0s}^{LJ} \rangle. \quad (24)$$

The calculation of other thermodynamic functions by perturbation theory requires more accurate definition of the perturbation potential to avoid including the strongly repulsive branch of the potential in the perturbation expansion.^[15] This problem has received much attention in the past.^[18] The Weeks-Chandler-Andersen (WCA)^[19] and Barker-Henderson (BH)^[16] schemes are most commonly applied, although some successful alternatives have been formulated as well.^[23,75,76]

All perturbation schemes for nonpolar solvation separate the LJ potential into the repulsive and attractive parts, with the pair distribution function of the repulsive part often approximated by that of a hard-sphere fluid.^[19] Since we have access, through MD simulations, to the ensemble configurations when the solute carries the entire LJ potential, we apply the λ -perturbation scheme instead. The long-ranged perturbation potential is chosen according to the Barker-Henderson protocol^[16]

$$u_{0s}^{BH} = u_{0s}^{LJ} \theta(r - r_c), \quad (25)$$

in which $\theta(x)$ is the Heaviside step function and the cutoff distance $r_c = \sigma = 3.33 \text{ \AA}$ is the LJ diameter for the carbon-oxygen solute-solvent interaction. The cutoff distance, therefore, sets up the radius of the hard-sphere reference potential u_{0s}^{HS} in Eq. (1) with $u_{0s}^{LJ} = u_{0s}^{BH}$ considered as the LJ perturbation potential.

The average $\langle u_{0s}^{BH} \rangle_\lambda$ in Eq. (4) can be written as

$$\langle u_{0s}^{BH} \rangle_\lambda = Q_\lambda^{-1} \int u_{0s}^{BH} e^{-\beta H_1 + \beta(1-\lambda)u_{0s}^{BH}} d\Gamma, \quad (26)$$

where Q_λ is the partition function corresponding to H_λ in Eq. (3) and $d\Gamma$ denotes integration over the system phase space. Since the ensemble statistics with the full Hamiltonian $H_1 = H_0 + u_{0s}^{BH}$ is available from the simulation trajectories, one can perform the perturbation expansion in Eqs. (3), (4) and (26) in the perturbation term $(1-\lambda)u_{0s}^{BH}$. The ensemble averages $\langle \dots \rangle = \langle \dots \rangle_1$ in the perturbation series then correspond the full LJ potential at $\lambda = 1$. By truncating the expansion after the second terms, one gets

$$\mu_{0s}^{LJ} = \langle u_{0s}^{BH} \rangle + (\beta/2) \langle (\delta u_{0s}^{BH})^2 \rangle. \quad (27)$$

Similarly, the correlation $\langle \delta u_{0s}^{BH} \delta U_{ss} \rangle_\lambda$ entering the solvent re-

Table 2 Thermodynamic solvation potentials^a for C_{60}^z at 300 K (the energies are in eV).

z	$-T_s^E$	$-e^E$	$-e_{0s}^E$ ^b	$-\mu_{0s}^E$ ^c	e_{ss}^E ^d	$-T_s^{LJ}$	$-e^{LJ}$	$-e_{0s}^{LJ}$	$-\mu_{0s}^{LJ}$ ^e	e_{ss}^{LJ}
1	0.07	0.71	1.53	0.64	0.82	0.16	2.54	2.35	2.38	-0.19
0	—	—	—	—	—	0.35	2.72	2.37	2.37	-0.35
-1	-0.39	0.82	2.33	1.21	1.51	0.3	2.61	2.29	2.31	-0.32
-2	0.01	4.57	9.73	4.56	5.15	-0.12	2.12	2.03	2.24	-0.09
-3	1.13	12.20	21.50	11.10	9.28	-0.69	1.61	1.83	2.3	0.21
-4	1.64	21.94	38.12	20.31	16.18	-1.32	1.11	1.48	2.43	0.36

^aElectrostatic component is calculated as extrapolation to $N \rightarrow \infty$ of the simulation results obtained at $N = 1200$ and $N = 2413$ water molecules in the simulation box. ^bCalculated from Eq. (18). ^cCalculated from Eqs. (14) and (15) applied to the electrostatic component of the solute-solvent interaction energy. ^dCalculated from Eq. (19). ^eCalculated from Eq. (27).

Table 3 Solvation heat capacities for C_{60}^z at 300 K.

z	C_V^E/k_B	$\Delta C_{ss}^E/k_B$ ^a	C_V^{LJ}/k_B ^b
1	169	248	19
-1	-67	72	30
-2	-296	149	5
-3	212	793	-31
-4	620	1553	-62

^aCalculated by subtracting $\beta^2 \langle \delta U_{ss}^2 \rangle$ for charged and neutral states at a given N (Eq. (23)), followed by extrapolation to $N \rightarrow \infty$. ^bCalculated from the first two terms in Eq. (30)

structuring energy in Eq. (9) is independent of λ in the lowest order of the perturbation theory^[15] and one gets

$$e_{ss}^{LJ} = -\beta \langle \delta u_{0s}^{BH} \delta U_{ss} \rangle. \quad (28)$$

From Eqs. (24)–(28), the following relation for the entropy of LJ solvation follows

$$T_s^{LJ} = \langle (u_{0s}^{LJ} - u_{0s}^{BH}) \rangle + e_{ss}^{LJ} - (\beta/2) \langle (\delta u_{0s}^{BH})^2 \rangle. \quad (29)$$

We find that the solute-solvent LJ energy e_{0s}^{LJ} is large (Table 2), but the entropy of solvation by LJ forces is relatively insignificant in the overall solvation thermodynamics.^[11,21,31,50,73,77] The same is true for the energy of solvent restructuring e_{ss}^{LJ} . This result for the LJ component of solvation is very distinct from the picture found for electrostatic solvation: in that case the low entropy of electrostatic solvation, which is comparable in the magnitude to that from LJ interactions, is the result of a nearly complete cancellation of two large in magnitude and opposite in sign energies through Eqs. (20) and (21).

By combining Eq. (29) with Eq. (11) for the solvation heat capacity, one obtains

$$C_V^{LJ} = -2s^{LJ} + T^{-1} \langle (u_{0s}^{LJ} - u_{0s}^{BH}) \rangle + \Delta C_{ss}^{LJ}. \quad (30)$$

Here, ΔC_{ss}^{LJ} is the change of the heat capacity of the solvent due to the attractive part of the LJ potential. In other words, this is the difference in the heat capacities of the solvent between the solution containing the repulsive solute and that with the full LJ potential. As we have mentioned above, the extensive, $\propto N$, component of the solvent heat capacity must cancel in the difference and only the intensive component should survive. Our MD simulations do not allow us to determine this component of the LJ

heat capacity and only the contribution of first two terms in Eq. (30) is listed in Table 3. Note that large contributions from water restructuring to the heat capacity of solvation reported in simulations of xenon^[78] included also the heat capacity of the cavity formation and not only that of LJ interactions considered here. The heat capacity due to LJ solvation is positive^[76,79] and small in magnitude compared to the electrostatic heat capacity, particularly for solutes carrying large charges (Table 3).

Returning to the question posed at the beginning of our discussion of whether the structural change in the interface is sensed by solvation thermodynamics, we see little evidence of that. The only notable result of the hydration shell's collapse at $z = -3, -4$ is the change in the sign of e_{ss}^{LJ} , s^{LJ} , and C_V^{LJ} compared to the solutes carrying lower charges (Tables 2 and 3). However, these changes of the nonpolar solvation thermodynamics are fully overshadowed by electrostatic solvation which follows the “trivial” linear response scaling with the solute charge without significant signatures produced by the change of the local structure.

Dynamics. In order to study the dynamics of the hydration shell, we have considered a number of time autocorrelation functions. The time correlation function of the electrostatic interaction energy u_{0s}^E captures the effect of the shell dynamics on the long-ranged solute-solvent interactions involving many water molecules on its decay length. The corresponding time correlation function is

$$C_E(t) = \langle \delta u_{0s}^E(t) \delta u_{0s}^E(0) \rangle. \quad (31)$$

The correlation function $C_{LJ}(t)$ is similarly defined with the replacement $u_{0s}^E \rightarrow u_{0s}^{LJ}$. This function is designed to be more sensitive to the local interfacial structure because of the short-range character of LJ interactions. Finally, the correlation function $C_1(t)$ of the order parameter $p_1(t)$ determined for the molecules in the first hydration shell reflects the single-molecule rotational dynamics altered by the solute-solvent interactions

$$C_1(t) = \langle \delta p_1(t) \delta p_1(0) \rangle. \quad (32)$$

Other dynamic correlation functions for single-molecule rotations can be defined^[9] and linked to one-particle dynamics measured by the NMR^[80] and infrared^[81,82] spectroscopies. We are not pursuing the goal of connecting to experimental data and instead are focused on the question of how the structural change of the interface, caused by altering the charge, affects the interfacial dynamics. From the dynamic data collected here, we consistently

Table 4 Average relaxation times $\langle\tau\rangle$ for the solute-solvent (Lennard-Jones (LJ) and electrostatic (E)) interactions and for the order parameter p_1 of the water molecules in the first hydration shell (relaxation times are in ps and E_a^s/k_B , $s = E, LJ$ are in K).

z	E^a	LJ^b	p_1^c	E_a^E/k_B	E_a^{LJ}/k_B
1	0.9	3.9	0.56	2412	2254
0	0.9	4.4	0.55		2192
-1	1.2	4.8	0.51	2236	2301
-2	1.2	3.4	0.54	2355	2533
-3	1.3	1.5	0.55	2478	2395
-4	1.7	0.9	0.72	2198	2226

^aRelaxation times $\langle\tau\rangle$ calculated from the time correlation function of electrostatic solute-solvent interaction as defined by Eq. (17). ^b $\langle\tau\rangle$ obtained from a multi-exponential fit of Eq. (31) upon replacing $u_{0s}^E \rightarrow u_{0s}^{LJ}$. ^c $\langle\tau\rangle$ determined from a multi-exponential fit of Eq. (32) (see the ESI[†]).

find very little sensitivity of the relaxation times to the charge of the solute and to the corresponding structural transition in the interface. This is particularly true when the long-range electrostatic interactions are concerned, while the dynamics of the short-range LJ interaction speeds up by a factor of ~ 4 when the solute charge changes from $z = \pm 1$ to $z = -4$. This alteration reflects changes in the density of the hydration shell, which, somewhat surprisingly, almost do not affect the dynamics of $p_1(t)$ (Table 4).

Relaxation times mostly independent on the charge state for fullerene are probably the consequence of the low charge density of these molecules. Even with collapse of the first hydration layer for $z = -3, -4$, the first peak of the oxygen RDF is at $r_O^{\max} > 6 \text{ \AA}$ (Table 1), significantly exceeding $r_O^{\max} \approx 2 \text{ \AA}$ for the Mg^{2+} cation.^[51] The parameter often employed to gauge the strength of ion-water electrostatic interaction in hydration thermodynamics^[65] and water exchange dynamics^[51] is the charge density $\propto z/[r_O^{\max}]^3$. For instance, water exchange time for Mg^{2+} is $\approx 130 - 664 \mu s$, while it is much lower, 117–753 ps, for Ca^{2+} characterized by $r_O^{\max} \approx 2.5 \text{ \AA}$. We obviously do not observe any such sensitivity of the dynamics to the selection of the ion, which indeed might be traced back to the low charge density of the fullerene ions.

The average relaxation times $\langle\tau\rangle$, obtained from multi-exponential fitting of the correlation functions, were calculated at different temperatures and fitted to the Arrhenius plots (Figs. S8 and S9 in the ESI[†])

$$\langle\tau\rangle = \tau_0 e^{\beta E_a}. \quad (33)$$

The activation energies E_a^s , $s = E, LJ$ are listed in Table 4.

The activation energy for the single-particle dynamics of bulk water^[81] is $E_a/k_B \simeq 2045 \text{ K}$. It is somewhat lower for SPC/E water, 1650 K,^[83] when calculated in the range of temperatures similar to that studied here. We, therefore, observe an increase of the activation barrier for the dynamics of hydration water (Table 4), but not as significant as reported ($\approx 70\%$) for the aqueous solution of tetramethylurea.^[81] Even though the activation barrier of water dynamics does not seem to correlate with the structural transition in the interface, it adds additional evidence^[84] against the geometric interpretation of the slower dynamics of water in

the hydration shell.^[85] The latter model anticipates that the volume excluded by the solute from the configurational space of the water molecule should lead to its slower dynamics. Such geometrical constraints, which are purely entropic, should not lead to a change in the activation barrier for reorientations, in contrast to experiment^[81] and our calculations listed in Table 4.

4 Discussion

Crossovers in thermodynamics of nonpolar solvation are often associated with the effect of the solute size on the network of water's hydrogen bonds enveloping the solute.^[59,86–89] Disruption of the hydrogen-bond network by sufficiently large solutes, $\sim 1 \text{ nm}$ in size, has been linked to the crossover from volume-dominated to surface-dominated solvation.^[10,44] Solvation of charged solutes was found to mostly follow the predictions of the linear response models.^[35,63,64] From this standpoint, since size is not varied in our study, no fundamental changes to the established picture of hydration thermodynamics, particularly in terms of new crossovers, are anticipated from charging the solute.

The results presented here challenge these expectations. While we confirm the validity of linear solvation in the entire range of charges from $z = +1$ to $z = -4$, we have discovered a dramatic alteration of the structure of the hydration shell around buckminsterfullerene C_{60} when its charge reach the values $z = -3, -4$ (a pre-transition is seen already at $z = -2$). The structural crossover of the hydration shell is characterized by a significant reduction of tetrahedral order, density collapse^[90] (shift of the distribution-function peak to closer distances), and disruption of the network of hydrogen bonds in the shell. Breaking hydrogen bonds allows waters to align along the local electric fields to produce orientational order in the hydration shell. The combination of reorientation of the water molecules with enhanced density forces the release of OH bonds pointing toward the solute (dangling bond^[58–60]). This phenomenology, involving broken network of hydrogen bonds, density enhancement, and build-up of orientated water domains is qualitatively similar to the picture observed for hydration shells of proteins.^[91,92] From a general perspective, our observations confirm that long-ranged and sufficiently strong interactions can cause structural transitions, but, because of their slow change and relatively weak forces, produce essentially no impact on the local dynamics. Therefore, measurements of the hydration-shell dynamics might not provide a sufficiently sensitive probe of the local structure and might not be able to signal the occurrence of a structural transition in the hydration shell.

The structural crossover observed here is unrelated to dewetting/drying transitions considered in relation to crossovers predicted to occur for water in contact with hydrophobic solutes.^[86–89] It is also essentially independent from temperature, in contrast to gradual transformations, with increasing temperature, of OH vibrational spectra of the shell changing frequency from below the frequency of bulk water to higher than in the bulk.^[48,59] The results reported here fall under the general umbrella of interfacial structural crossovers induced by the solute-solvent electrostatics. We have previously observed similar structural changes induced by surface solvation of dipoles placed at the

outer layer of the solute^[70] and due to an increased polarizability of the solute causing thermodynamic instability of the interfacial dipolar polarization.^[90] In the case of instability driven by the solute polarizability, an increased population of interfacial dangling OH bonds was found, in a general agreement with the new results reported here.

We find that all thermodynamic functions describing electrostatic solvation scale quadratically with the solute charge, as expected from linear solvation models. The entropy of electrostatic solvation is negative and is relatively small in magnitude as a result of nearly complete mutual cancellation^[11] between the solvation chemical potential and the energy of solvent restructuring e_{ss} in Eq. (20). Given this physical origin of the electrostatic solvation entropy, it is hardly conceivable that continuum dielectric models can be reliable for entropy estimates. Critical tests of the Born model of ionic solvation is often hampered by the unknown radius of the dielectric cavity considered as a fitting parameter.^[93] The cavity radius, however, cancels out in the ratio of the entropy and chemical potential of solvation, which in the Born model becomes

$$\frac{T_s^E}{\mu_{0s}^E} = -\frac{1}{\epsilon(\epsilon-1)} \frac{\partial \epsilon}{\partial T}, \quad (34)$$

where $\epsilon(T)$ is the temperature-dependent dielectric constant. For SPC/E water studied here one has^[94] $\epsilon(300\text{ K}) = 70.1$ and $\partial\epsilon/\partial T \simeq -0.058\text{ K}^{-1}$. With these numbers, one gets $T_s^E/\mu_{0s}^E \simeq 3.6 \times 10^{-3}$ from Eq. (34), while a much higher value $\simeq 0.1$ follows for the same ratio in Table 2. It is clear that the Born model severely underestimates the entropy of electrostatic solvation.^[69,93,95,96]

The inability of continuum models to describe the entropy of solvation has very practical consequences to a number of problems in biophysics. The pKa values of protein residues are often estimated by using continuum electrostatic models and those calculations cannot capture the effect of temperature. Obviously, the heat capacity, the second derivative of the electrostatic free energy of solvation, cannot be approached by continuum-based calculations. The heat capacity is, however, an important parameter for both protein folding^[97–99] and enzyme catalysis.^[100] For the latter, heat capacities of activation (the difference of heat capacities in the activated and reactant states) are often negative, producing upward-curved Arrhenius plots.^[100] Electrostatics significantly affects activation barriers of enzymatic reactions.^[101] Therefore, given the results obtained in this study (Table 3), negative activation heat capacities imply stronger electrostatic solvation (Eq. (22)) if the change in the heat capacity of the solvent does not apply to the active site. This outcome is in line with the accepted view that electrostatic stabilization is reached in the transition state,^[101] as an extension of Pauling's idea^[102] of tighter binding in the activated state of the catalytic site.^[103]

A positive electrostatic heat capacity for the cation ($z = +1$, Table 3) found here is in qualitative agreement with previous calculations.^[36] Hydration of cations is also lower in the absolute magnitude of the chemical potential than hydration of anions.^[66,67] There is, therefore, a thermodynamic driving force to place more

anions to the surface of a folded protein to increase its stabilization energy and solubility. This thermodynamic preference should produce a negative heat capacity of folding due to the different signs of heat capacities of electrostatic hydrations for cations and anions. This is indeed a well documented and universal observation for thermodynamics of protein folding.^[98,99] We also find that solvation heat capacities from electrostatics far exceed those from LJ solute-solvent interactions pointing to the dominance of electrostatic interactions in the heat capacity of solvation and, potentially, in thermodynamics of protein collapse/folding.^[104] In agreement with this view, a recent single-molecule study has shown^[105] that temperature-induced collapse of an intrinsically-disordered protein is driven by the temperature-dependent hydration free energies of the hydrophilic residues and not by the anticipated hydrophobic effect.

Acknowledgements. This research was supported by the National Science Foundation (CHE-1800243). CPU time was provided by the National Science Foundation through XSEDE resources (TG-MCB080071). We greatly benefited from discussions with Dor Ben-Amotz.

References

- 1 Stanley, H. E. *Introduction to phase transitions and critical phenomena* (Oxford University Press, New York, 1987).
- 2 Gonzalo, J. A. *Effective field approach to phase transitions and some applications to ferroelectrics* (World Scientific, Singapore, 1991).
- 3 Angell, C. A. Formation of glasses from liquids and biopolymers. *Science* **267**, 1924–1935 (1995).
- 4 Adam, G. & Gibbs, J. H. On the temperature dependence of cooperative relaxation properties in glass-forming liquids. *J. Chem. Phys.* **43**, 139–146 (1965).
- 5 Debenedetti, P. G. & Stillinger, F. H. Supercooled liquids and glass transitions. *Nature* **410**, 259–267 (2001).
- 6 Lubchenko, V. & Wolynes, P. G. Theory of Structural Glasses and Supercooled Liquids. *Ann. Rev. Phys. Chem.* **58**, 235–266 (2007).
- 7 Berthier, L. *et al.* Direct experimental evidence of a growing length scale accompanying glass transition. *Science* **310**, 1797–1800 (2005).
- 8 Bakker, H. J. & Skinner, J. L. Vibrational Spectroscopy as a Probe of Structure and Dynamics in Liquid Water. *Chem. Rev.* **110**, 1498–1517 (2010).
- 9 Laage, D., Stirnemann, G., Sterpone, F., Rey, R. & Hynes, J. T. Reorientation and allied dynamics in water and aqueous solutions. *Annu. Rev. Phys. Chem.* **62**, 395–416 (2011).
- 10 Chandler, D. Interfaces and the driving force of hydrophobic assembly. *Nature* **437**, 640–647 (2005).
- 11 Ben-Amotz, D. & Underwood, R. Unraveling water's entropic mysteries: A unified view of non-polar, polar and ionic hydration. *Acc. Chem. Res.* **41**, 957–967 (2008).
- 12 Hansen, J.-P. & McDonald, I. R. *Theory of Simple Liquids* (Academic Press, Amsterdam, 2013), 4 edn.
- 13 Hummer, G. & Szabo, A. Calculation of free-energy differ-

- ences from computer simulations of initial and final states. *J. Chem. Phys.* **105**, 2004–2010 (1996).
- 14 Zwanzig, R. W. High-temperature equation of state by a perturbation method. I. Nonpolar gases. *J. Chem. Phys.* **22**, 1420–1426 (1954).
- 15 Gray, C. G. & Gubbins, K. E. *Theory of Molecular Liquids* (Clarendon Press, Oxford, 1984).
- 16 Barker, J. A. & Henderson, D. What is 'liquid'? Understanding the states of matter. *Rev. Mod. Phys.* **48**, 587–671 (1976).
- 17 Ailawadi, N. K. Equilibrium theories of simple liquids. *Phys. Rep.* **57**, 241–306 (1980).
- 18 Zhou, S. & Solana, J. R. Progress in the perturbation approach in fluid and fluid-related theories. *Chem. Rev.* **109**, 2829–2858 (2009).
- 19 Andersen, H. C., Chandler, D. & Weeks, J. D. Roles of repulsive and attractive forces in liquids: The equilibrium theory of classical fluids. *Adv. Chem. Phys.* **34**, 105–155 (1976).
- 20 Gallicchio, E., Kubo, M. M. & Levy, R. M. Enthalpy-entropy and cavity decomposition of alkane hydration free energies: Numerical results and implications for theories of hydrophobic solvation. *J. Phys. Chem. B* **104**, 6271–6285 (2000).
- 21 Huang, D. M. & Chandler, D. The hydrophobic effect and the influence of solute-solvent attractions. *J. Phys. Chem. B* **106**, 2047–2053 (2002).
- 22 Harris, R. C. & Pettitt, B. M. Reconciling the understanding of 'hydrophobicity' with physics-based models of proteins. *J. Phys.: Condens. Matter* **28**, 083003–14 (2016).
- 23 Paricaud, P. A general perturbation approach for equation of state development: Applications to simple fluids, ab initio potentials, and fullerenes. *J. Chem. Phys.* **124**, 154505–18 (2006).
- 24 Widom, B. Some topics in the theory of fluids. *J. Chem. Phys.* **39**, 2808–2812 (1963).
- 25 Yu, H.-A. & Karplus, M. A thermodynamic analysis of solvation. *J. Chem. Phys.* **89**, 2366 (1988).
- 26 Guillot, B. & Guissani, Y. A computer simulation study of the temperature dependence of the hydrophobic hydration. *J. Chem. Phys.* **99**, 8075–8094 (1993).
- 27 Lee, B. Enthalpy-entropy compensation in the thermodynamics of hydrophobicity. *Biophys. Chem.* **51**, 271–278 (1994).
- 28 Marcus, R. A. Electrostatic free energy and other properties of states having nonequilibrium polarization. I. *J. Chem. Phys.* **24**, 979–989 (1956).
- 29 Ghorai, P. K. & Matyushov, D. V. Solvent reorganization entropy of electron transfer in polar solvents. *J. Phys. Chem. A* **110**, 8857–8863 (2006).
- 30 Ben-Amotz, D. & Widom, B. Generalized solvation heat capacities. *J. Phys. Chem. B* **110**, 19839–19849 (2006).
- 31 Ben-Amotz, D. Global thermodynamics of hydrophobic cavitation, dewetting, and hydration. *J. Chem. Phys.* **123**, 184504–9 (2005).
- 32 Chandler, D. Gaussian field model of fluids with an application to polymeric fluids. *Phys. Rev. E* **48**, 2898–2905 (1993).
- 33 Ashbaugh, H. S. & Pratt, L. R. Colloquium: Scaled particle theory and the length scales of hydrophobicity. *Rev. Mod. Phys.* **78**, 159–178 (2006).
- 34 Phillips, J. C. *et al.* Scalable molecular dynamics with NAMD. *J. Comput. Chem.* **26**, 1781–1802 (2005).
- 35 Rajamani, S., Ghosh, T. & Garde, S. Size dependent ion hydration, its asymmetry, and convergence to macroscopic behavior. *J. Chem. Phys.* **120**, 4457–4466 (2004).
- 36 Sedlmeier, F. & Netz, R. R. Solvation thermodynamics and heat capacity of polar and charged solutes in water. *J. Chem. Phys.* **138**, 115101–13 (2013).
- 37 Choudhury, N. A molecular dynamics simulation study of buckyballs in water: Atomistic versus coarse-grained models of C₆₀. *J. Chem. Phys.* **125**, 034502–8 (2006).
- 38 Varanasi, S. R., Guskova, O. A., John, A. & Sommer, J. U. Water around fullerene shape amphiphiles: A molecular dynamics simulation study of hydrophobic hydration. *J. Chem. Phys.* **142**, 224308–16 (2015).
- 39 Shen, Y. R. & Ostroverkhov, V. Sum-frequency vibrational spectroscopy on water interfaces: Polar orientation of water molecules at interfaces. *Chem. Rev.* **106**, 1140–1154 (2006).
- 40 Velasco-Velez, J.-J. *et al.* Interfacial water. The structure of interfacial water on gold electrodes studied by x-ray absorption spectroscopy. *Science* **346**, 831–834 (2014).
- 41 Pedroza, L. S., Brandimarte, P., Rocha, A. R. & Fernández-Serra, M. V. Bias-dependent local structure of water molecules at a metallic interface. *Chem. Sci.* **9**, 62–69 (2018).
- 42 Kimura, K. *et al.* Visualizing water molecule distribution by atomic force microscopy. *J. Chem. Phys.* **132**, 194705–6 (2010).
- 43 Kageshima, M. Layer-resolved relaxation dynamics of confined water analyzed through subnanometer shear measurement. *EPL (Europhysics Letters)* **107**, 66001–7 (2014).
- 44 Rensing, R. C. & Weeks, J. D. Dissecting Hydrophobic Hydration and Association. *J. Phys. Chem. B* **117**, 15479–15491 (2013).
- 45 Matubayasi, N. Matching-mismatching of water geometry and hydrophobic hydration. *J. Am. Chem. Soc.* **116**, 1450–1456 (1994).
- 46 Chau, P. L. & Hardwick, A. J. A new order parameter for tetrahedral configurations. *Mol. Phys.* **93**, 511–518 (1998).
- 47 Errington, J. R. & Debenedetti, P. G. Relationship between structural order and the anomalies of liquid water. *Nature* **409**, 318–321 (2001).
- 48 Wu, X., Lu, W., Streacker, L. M., Ashbaugh, H. S. & Ben-Amotz, D. Temperature-dependent hydrophobic crossover length scale and water tetrahedral order. *J. Phys. Chem. Lett.* **9**, 1012–1017 (2018).
- 49 Zhang, C. & Galli, G. Dipolar correlations in liquid water. *J. Chem. Phys.* **141**, 084504 (2014).
- 50 Kim, J., Tian, Y. & Wu, J. Thermodynamic and structural evidence for reduced hydrogen bonding among water molecules near small hydrophobic solutes. *J. Phys. Chem. B*

- 119, 12108–12116 (2015).
- 51 Lee, Y., Thirumalai, D. & Hyeon, C. Ultrasensitivity of water exchange kinetics to the size of metal ion. *J. Am. Chem. Soc.* **139**, 12334–12337 (2017).
- 52 Luzar, A. & Chandler, D. Effect of environment on hydrogen bond dynamics in liquid water. *Phys. Rev. Lett.* **76**, 928–931 (1996).
- 53 Silverstein, K. A. T., Haymet, A. D. J. & Dill, K. A. The Strength of Hydrogen Bonds in Liquid Water and Around Nonpolar Solutes. *J. Am. Chem. Soc.* **122**, 8037–8041 (2000).
- 54 Graziano, G. & Lee, B. On the intactness of hydrogen bonds around nonpolar solutes dissolved in water. *J. Phys. Chem. B* **109**, 8103–8107 (2005).
- 55 Keshri, S. & Tembe, B. L. Thermodynamics of hydration of fullerenes [C₆₀(OH)_n] and hydrogen bond dynamics in their hydration shells. *J. Chem. Phys.* **146**, 074501–15 (2017).
- 56 Remsing, R. C. *et al.* Water lone pair delocalization in classical and quantum descriptions of the hydration of model ions. *J. Phys. Chem. B* **122**, 3519–3527 (2018).
- 57 Lee, C. Y., McCammon, J. A. & Rossky, P. J. The structure of liquid water at an extended hydrophobic surface. *J. Chem. Phys.* **80**, 4448–4455 (1984).
- 58 McFearnin, C. L., Beaman, D. K., Moore, F. G. & Richmond, G. L. From Franklin to today: Toward a molecular level understanding of bonding and adsorption at the oil-water interface. *J. Phys. Chem. C* **113**, 1171–1188 (2008).
- 59 Davis, J. G., Rankin, B. M., Gierszal, K. P. & Ben-Amotz, D. On the cooperative formation of non-hydrogen-bonded water at molecular hydrophobic interfaces. *Nat. Chem.* **5**, 796–802 (2013).
- 60 Zukowski, S. R., Mitev, P. D., Hermansson, K. & Ben-Amotz, D. CO₂ Hydration shell structure and transformation. *J. Phys. Chem. Lett.* **8**, 2971–2975 (2017).
- 61 Ben-Amotz, D., Raineri, F. O. & Stell, G. Solvation thermodynamics: Theory and applications. *J. Phys. Chem. B* **109**, 6866–6878 (2005).
- 62 Hummer, G., Pratt, L. R., García, A. E., Berne, B. J. & Rick, S. W. Electrostatic potentials and free energies of solvation of polar and charged molecules. *J. Phys. Chem. B* **101**, 3017–3020 (1997).
- 63 Hummer, G., Pratt, L. R. & García, A. E. Ion Sizes and Finite-Size Corrections for Ionic-Solvation Free Energies. *J. Chem. Phys.* **107**, 9275–9277 (1997).
- 64 Åqvist, J. & Hansson, T. On the validity of electrostatic linear response in polar solvents. *J. Phys. Chem.* **100**, 9512–9521 (1996).
- 65 Collins, K. D. Charge density-dependent strength of hydration and biological structure. *Biophys. J.* **72**, 65–76 (1997).
- 66 Reif, M. M. & Hünenberger, P. H. Origin of asymmetric solvation effects for ions in water and organic solvents investigated using molecular dynamics simulations: The Swain acidity–basicity scale revisited. *J. Phys. Chem. B* **120**, 8485–8517 (2016).
- 67 Duignan, T. T., Baer, M. D., Schenter, G. K. & Mundy, C. J. Electrostatic solvation free energies of charged hard spheres using molecular dynamics with density functional theory interactions. *J. Chem. Phys.* **147**, 161716–12 (2017).
- 68 Scheu, R. *et al.* Specific ion effects in amphiphile hydration and interface stabilization. *J. Am. Chem. Soc.* **136**, 2040–2047 (2014).
- 69 Matyushov, D. V. & Ladanyi, B. M. A perturbation theory and simulations of the dipole solvation thermodynamics: Dipolar hard spheres. *J. Chem. Phys.* **110**, 994–1009 (1999).
- 70 Friesen, A. D. & Matyushov, D. V. Surface polarity and nanoscale solvation. *J. Phys. Chem. Lett.* **3**, 3685–3689 (2012).
- 71 Southall, N. T., Dill, K. A. & Haymet, A. D. J. A view of the hydrophobic effect. *J. Phys. Chem. B* **106**, 521–533 (2002).
- 72 Stell, G. Fluids with long-range forces; Toward a simple analytic theory. In Berne, B. J. (ed.) *Statistical Mechanics. Part A: Equilibrium Techniques* (Plenum, New York, 1977).
- 73 Matyushov, D. V. & Schmid, R. A thermodynamic analysis of solvation in dipolar liquids. *J. Chem. Phys.* **105**, 4729 (1996).
- 74 Hedwig, G. R. & Hakin, A. W. Partial molar volumes and heat capacities of single ions in aqueous solution over the temperature range 288.15 to 328.15 K. *Phys. Chem. Chem. Phys.* **6**, 4690–11 (2004).
- 75 Ben-Amotz, D. & Stell, G. Hard sphere perturbation theory for fluids with soft-repulsive-core potentials. *J. Chem. Phys.* **120**, 4844–4851 (2004).
- 76 van Westen, T. & Gross, J. A critical evaluation of perturbation theories by Monte Carlo simulation of the first four perturbation terms in a Helmholtz energy expansion for the Lennard-Jones fluid. *J. Chem. Phys.* **147**, 014503–16 (2017).
- 77 Graziano, G. Hydration entropy of polar, nonpolar and charged species. *Chem. Phys. Lett.* **479**, 56–59 (2009).
- 78 Paschek, D. Heat capacity effects associated with the hydrophobic hydration and interaction of simple solutes: A detailed structural and energetical analysis based on molecular dynamics simulations. *J. Chem. Phys.* **120**, 10605–10617 (2004).
- 79 Baldwin, R. L. Temperature dependence of the hydrophobic interaction in protein folding. *Proc. Natl. Acad. Sci. USA* **83**, 8069–8072 (1986).
- 80 Halle, B. Protein hydration dynamics in solution: a critical survey. *Phil. Trans. R. Soc. Lond.* **359**, 1207–1224 (2004).
- 81 Petersen, C., Tielrooij, K. J. & Bakker, H. J. Strong temperature dependence of water reorientation in hydrophobic hydration shells. *J. Chem. Phys.* **130**, 214511–7 (2009).
- 82 Strazdaite, S., Versluis, J. & Bakker, H. J. Water orientation at hydrophobic interfaces. *J. Chem. Phys.* **143**, 084708 (2015).
- 83 Ghorai, P. K. & Matyushov, D. V. Solvent reorganization energy in solvents above the glass transition. *J. Phys. Chem. B* **110**, 1866–1871 (2006).
- 84 Stirnemann, G. *et al.* Non-monotonic dependence of wa-

- ter reorientation dynamics on surface hydrophilicity: competing effects of the hydration structure and hydrogen-bond strength. *Phys. Chem. Chem. Phys.* **13**, 19911–19917 (2011).
- 85 Laage, D., Stirnemann, G. & Hynes, J. T. Why water reorientation slows without iceberg formation around hydrophobic solutes. *J. Phys. Chem. B* **113**, 2428–2435 (2009).
- 86 Stillinger, F. H. Structure in aqueous solutions of nonpolar solutes from the standpoint of scaled-particle theory. *J. Solut. Chem.* **2**, 141–158 (1973).
- 87 Lum, K., Chandler, D. & Weeks, J. Hydrophobicity at small and large length scales. *J. Phys. Chem. B* **103**, 4570–4577 (1999).
- 88 Garde, S., Hummer, G., García, A. E., Paulaitis, M. E. & Pratt, L. R. Origin of entropy convergence in hydrophobic hydration and protein folding. *Phys. Rev. Lett.* **77**, 4966–4968 (1996).
- 89 Rajamani, S., Truskett, T. M. & Garde, S. Hydrophobic hydration from small to large lengthscales: Understanding and manipulating the crossover. *Proc. Natl. Acad. Sci.* **102**, 9475–9480 (2005).
- 90 Dinpajoo, M. & Matyushov, D. V. Interfacial structural transition in hydration shells of a polarizable solute. *Phys. Rev. Lett.* **114**, 207801 (2015).
- 91 Bellissent-Funel, M.-C. *et al.* Water determines the structure and dynamics of proteins. *Chem. Rev.* **116**, 7673–7697 (2016).
- 92 Martin, D. R. & Matyushov, D. V. Dipolar nanodomains in protein hydration shells. *J. Phys. Chem. Lett.* **6**, 407–412 (2015).
- 93 Dinpajoo, M. & Matyushov, D. V. Free energy of ion hydration: Interface susceptibility and scaling with the ion size. *J. Chem. Phys.* **143**, 044511 (2015).
- 94 Fennell, C. J., Li, L. & Dill, K. A. Simple liquid models with corrected dielectric constants. *J. Phys. Chem. B* **116**, 6936–6944 (2012).
- 95 Roux, B., Yu, H.-A. & Karplus, M. Molecular basis for the Born model of ion solvation. *J. Phys. Chem.* **94**, 4683–4688 (1990).
- 96 Lynden-Bell, R. M. & Rasaiah, J. C. From hydrophobic to hydrophilic behaviour: A simulation study of solvation entropy and free energy of simple solutes. *J. Chem. Phys.* **107**, 1981–1991 (1997).
- 97 Cooper, A. Protein fluctuations and the thermodynamic uncertainty principle. *Prog. Biophys. Molec. Biol.* **44**, 181–214 (1984).
- 98 Prabhu, N. V. & Sharp, K. A. Heat capacity of proteins. *Annu. Rev. Phys. Chem.* **56**, 521–548 (2005).
- 99 Cooper, A. Protein heat capacity: An anomaly that maybe never was. *J. Phys. Chem. Lett.* **1**, 3298–3304 (2010).
- 100 Arcus, V. L. *et al.* On the temperature dependence of enzyme-catalyzed rates. *Biochemistry* **55**, 1681–1688 (2016).
- 101 Warshel, A., Sharma, P. K., Kato, M. & Parson, W. W. Modeling electrostatic effects in proteins. *Biochim. Biophys. Acta* **1764**, 1647–1676 (2006).
- 102 Pauling, L. Molecular architecture and biological reactions. *Chem. Eng. News* **24**, 1375–1377 (1946).
- 103 Nagel, Z. D. & Klinman, J. P. A 21st century revisionist's view at a turning point in enzymology. *Nat. Chem. Biol.* **5**, 543–550 (2009).
- 104 Ben-Naim, A. *Molecular Theory of Water and Aqueous Solutions: Understanding Water* (World Scientific Publishing Co Pte Ltd, 2014).
- 105 Wuttke, R. *et al.* Temperature-dependent solvation modulates the dimensions of disordered proteins. *Proc. Natl. Acad. Sci. USA* **111**, 5213–5218 (2014).